Phys. Med. Biol. **45** (2000) 1141–1150. Printed in the UK PII: S0031-9155(00)08032-5

Effect of myocardial anisotropy on the torso current flow patterns, potentials and magnetic fields*

Ceon Ramon†, Yanqun Wang‡, Jens Haueisen§, Paul Schimpf‖, S Jaruvatanadilok† and A Ishimaru†

† Department of Electrical Engineering, Box 352 500, University of Washington, Seattle, WA 98195, USA

‡ Rosetta Inpharmatics, Inc., Kirkland, WA 98034, USA

§ Biomagnetics Center, F S University, Jena, Germany

‖ Department of Computer Science, Eastern Washington University, Cheney, WA, USA

E-mail: ceon@u.washington.edu

Received 21 September 1999, in final form 6 January 2000

Abstract. The effects of myocardial anisotropy on the torso current flow patterns, voltage and the magnetic field were examined using an anatomically realistic torso model of an adult male subject. A finite element model of the torso was built with 19 major tissue types identified. The myocardial fibre orientation in the heart wall was included with a voxel resolution of $0.078 \times 0.078 \times 0.3$ cm. The fibre orientations from the canine heart which are available in the literature were mapped to our adult male subject's human heart using deformable mapping techniques. The current and potential distribution in the whole torso were computed using an idealized dipolar source of ± 1.0 V in the middle of the septum of the heart wall as a boundary condition. An adaptive finite element solver was used. Two cases were studied. In one case the myocardium was isotropic and in the other it was anisotropic. It was found that the current density distribution shows a very noticeable difference between the isotropic and anisotropic myocardium. The resultant magnetic field in front of the torso was computed using the Biot–Savart law. It was found that the magnetic field profile was slightly affected by the myocardial anisotropy. The potential on the torso surface also shows noticeable changes due to the myocardial anisotropy.

1. Introduction

It has been suggested that the geometry of the myocardial fibres can affect the current flow patterns in the heart wall (Plonsey 1974, Streeter 1979). This will change the volume current flow patterns in the heart and subsequently also in the torso. It will also affect the surface torso potentials and the torso magnetic fields, which need to be examined with computer simulations using a realistic heart–torso model. There are numerous previous studies available in the literature that examine the effect of myocardial tissue anisotropy on the epicardial and torso potentials, and also on wavefront propagation in the heart wall. Wei *et al* (1995a, b) have examined the effect of anisotropy on the heart excitation and on the body surface electrocardiograms. They did not observe any significant difference for a normal heart which could be due to the simpler, low resolution model of the torso. Thivierge *et al* (1997) studied the effect of myocardial anisotropy with equivalent heart dipoles. Their hypothesis was that

* This work was supported in part by the National Science Foundation INT-9726712, NIH grant R55 RR13301, and an equipment grant from the Seattle Foundation.

0031-9155/00/051141+10$30.00

inclusion of anisotropy adds an axial dipole component oriented along the fibres. They found that volume conductor conductivities close to that of torso conductivities diminished the dipoles oriented along the fibres. This would imply that myocardial anisotropy did not show a strong influence in the case where the volume conductor conductivities are similar to the torso conductivities.

In an earlier study (Schmidt and Pilkington 1991), using spherical models of heart and torso, it was concluded that myocardial anisotropy has a significant effect on the magnitude of the body surface potentials. A recent review article (Taccardi *et al* 1997) suggested that myocardial fibre structure plays an important role in the electrical activity of the myocardium. In addition, computer models of the heart are available (Huiskamp 1998, Lorange and Gularjani 1993, Siregar *et al* 1998) which include myocardial tissue anisotropy. These computer models have been used to simulate the epicardial potentials and electrocardiograms but have not been used to quantify the effects of myocardial anisotropy. Also, the effect of myocardial anisotropy on the torso magnetic fields, to our knowledge, has not been studied before.

For detailed accounting of the flow of the volume currents in the heart and torso one needs a realistic heterogeneous model of the whole torso in which all the major tissue types have been identified (Czapski *et al* 1996, 1998, Ramon *et al* 1998, Schimpf *et al* 1998). Similar models would also be needed to study the effects of myocardial tissue anisotropy on the current flow patterns in the torso. Using such a model, we studied the changes in the current flow patterns and found that they are significantly affected by the anisotropy. These findings suggest that the orientation of the cardiac muscle fibres should be included in the heart–torso models for an accurate modelling of the volume current distribution in the heart and torso, and also for improved modelling of the torso potentials and magnetic fields. Details of our methods, results and a discussion are given in the following sections.

2. Methods

2.1. Torso model

Our procedures for building the heart–torso model and for computing the current distribution and the magnetic field profiles are described elsewhere (Czapski *et al* 1996, Ramon *et al* 1998, Schimpf *et al* 1998). A brief review of our methods is given here. We used magnetic resonance imaging (MRI) data of an adult male subject without any known heart problems to construct a high resolution model of the heart and torso. MRI data were collected at the University of Washington Medical Center, Seattle, WA with a GE Signa 1.5 T MRI machine. Each proton density MRI slice was collected with cardiac gating to reduce the motion artefacts. The MRI data were collected when the heart was in the diastolic state. The entire scan consisted of 52 transaxial slices with 6 mm vertical separation. Each slice has a 256 × 256 pixel resolution. In order to increase vertical resolution of the model, an additional 51 images were generated between the original slices by linear interpolation, resulting in a total of 103 images with 3 mm vertical separation. Similarly resolution in each slice was increased to 512 × 512 pixels by using bicubic interpolation. This was done to provide a better resolution for image segmentation and later on for insertion of the electrical sources in the finite element model of the heart. The field of view in the GE MRI machine was 40 × 40 cm. This gives us a pixel resolution of 0.078 × 0.078 cm for the images of 512 × 512 pixels. Semi-automatic tissue classification software was used to segment images. Nineteen different tissue types were identified in the whole torso.

A layout of the torso surface, coordinate orientation and the sampling surface in which the magnetic field profiles were computed is shown in figure 1(*a*). A detailed schematic diagram of the heart wall, the image slices in the heart and the location of the dipoles are shown in

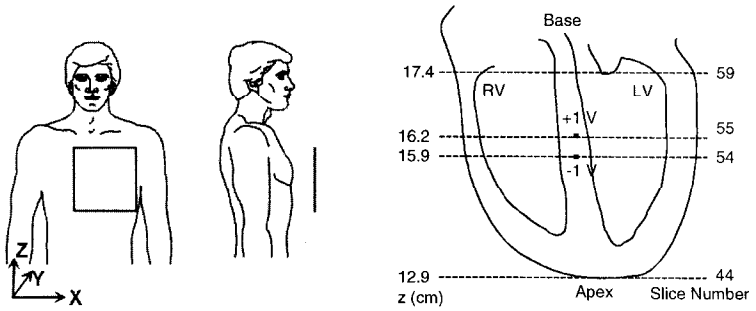

Figure 1. (*a*) A layout of the torso shape, the orientation of the coordinate system and the location of the planar sampling surface for the magnetic fields. (*b*) Details of the image slices in the heart area and the location of the dipolar source.

figure 1(*b*). The increasing x direction is from the right side of the subject to the left; the increasing y direction is from front (anterior) to the back (posterior) of the subject; and the increasing z direction is from the abdomen (inferior) to the shoulders (superior). The first image slice of the torso, i.e. slice number 1, is located at $z = 0$ cm at the upper abdomen area. The last image slice, i.e. slice number 103, is located at $z = 102 \times 0.3 = 30.6$ cm at the upper chest area. As shown in figure 1(*b*), the bottom of the heart, i.e. the apex, is located in slice number 44 at $z = 12.9$ cm. The top of the ventricles are in slice number 59, and the top of the heart is located in slice number 67 at $z = 19.8$ cm, which is not shown in the figure.

2.2. *Fibre mapping*

A complete data set of ventricular fibre orientation for the human heart is unavailable in the literature. However, it has been found that heart fibre structure is very similar across various mammalian species (Streeter 1979). A complete data set of the fibre orientation in a canine heart has been mapped at the University of Auckland, New Zealand (Nielson *et al* 1991), and it is available at their website on the Internet. This data set is being used by other research groups for incorporating the fibre anisotropy into computer models of the heart (Wang 1999, Eason *et al* 1998). We mapped the fibre orientations from the canine heart to our adult male subject's human heart using deformable mapping techniques (Wang 1999, Foley 1995).

The procedure consists of differentially deforming the shape of one heart to another and then interpolating the fibre orientation from one heart (source heart) to the other (target heart). Here the source heart is the dog heart for which fibre geometry data are available. The target heart is the human subject's heart to which we want to map the fibre geometry. Details of this procedure are given in Wang (1999). To facilitate the deformation of one heart shape to the other, landmark points are used. These landmark points are chosen at the corresponding anatomical sites of both hearts. These are well defined anatomical landmark points, such as points on the epicardium, left ventricular (LV) wall and right ventricular (RV) wall. We used AVS software to display the 3D shape of the dog heart and the shape of the human subject's heart in two different display windows. By visual inspection the corresponding landmark points were identified and tabulated for both hearts. We used a total of 96 landmark points on each heart. These points were evenly distributed, 32 points on the epicardial surface, 32 points on the LV endocardial wall and 32 points on the RV endocardial wall. We found that these

evenly distributed 96 landmark points were sufficient for mapping the morphology of the one heart to the other. However, one could use fewer or more landmark points, as needed, to map the morphology. These landmark points were then used to develop a geometric mapping function between the two hearts which was then used to interpolate the orientation of the fibres in the dog's heart to the human subject's heart. Using this procedure, the myocardial fibre orientation was estimated in each voxel of the heart wall of the human subject. This information was then included in the finite element model of the torso for solving the potential and current distribution in the whole torso.

2.3. Computational details

A finite element mesh with hexahedral (brick-shaped) elements was generated in the whole torso. We used the smallest elements of the size $0.078 \times 0.078 \times 0.3$ cm in the heart wall and larger size elements in other parts of the torso. An adaptive finite element solver developed by us was used for all the computational work (Schimpf *et al* 1996, 1998). A dipole of +1 and -1 V was placed between slices 55 and 54 in the septum. The exact location of the dipole is: +1 V at the pixel coordinate (259, 209) in slice number 55, and -1 V at the same pixel coordinate in slice number 54. This gives us a dipole of ± 1.0 V in the middle portion of the septum of the heart wall. This is an idealized dipole for computer simulations only and it does not represent any cardiac activation. Choice of ± 1.0 V was used so that computed results can be easily scaled to other values.

The potential and current distribution in the whole torso was computed for two cases using the dipole as a boundary condition. In one case we used the anisotropic myocardial tissue resistivities and in the other case the isotropic myocardial tissue resistivities. Isotropic tissue resistivities were used for all other tissue types and were kept the same in both cases. These resistivity values are available in the literature (Foster and Schwan 1989, Geddes and Baker 1967, Rush *et al* 1962) and have been used previously by us (Czapski *et al* 1996, Ramon *et al* 1998). All tissue resistivity and conductivity values used in our model are given in table 1. The resistivity values of myocardium are: isotropic myocardium, 420; anisotropic myocardium, 131.5 along the fibre direction and 758 transverse to the fibre direction. All resistivity values are in units of Ω cm.

Using the Biot–Savart law, the magnetic field outside the torso was computed from the primary currents flowing in the dipolar source and secondary volume currents in the whole torso. The magnetic field profiles were computed in a planar sampling surface located 1.0 cm in front (anterior) of the torso of the subject. The size of the sampling surface is 20×20 cm and the sampling points were on a 40×40 grid. This gives a grid spacing of 0.5×0.5 cm. A layout of the sampling surface is shown in figure 1(*a*). The sampling surface extends from 5 to 25 cm in the z direction and from 11 to 31 cm in the x direction.

All computations were performed on an Intel Pentium II, 350 MHz, 2 CPU, 512 MB memory workstation running a Linux operating system. An average run took about 30 min for computing the potential and current distribution in the whole torso. The post-processing and visualization of the data were done using Matlab 5.3 software (Mathworks, Inc., Natick, MA).

3. Results

3.1. Torso current flow patterns

The current density (μA cm^{-2}) distribution in a slice is shown in figure 2. Slice number 59 was chosen for showing the current distribution. It is four slices above the dipolar source.

Table 1. Conductivity/resistivity values of the major tissue types used in the computer model of heart and torso.

Tissue type	Conductivity (mS cm^{-1})	Resistivity (Ω cm)
Lungs	0.667	1500
Muscle	1.43	700
Fat	0.4	2500
Connective tissue	2.22	450
Liver	1.2	834
Stomach	1.25	800
Blood	6.49	154
Bone	0.0625	16 000
Isotropic myocardium	2.38	420
Anisotropic myocardium		
along fibre direction	7.604	131.5
transverse to fibre direction	1.319	758
Spleen	0.1	10 000
Soft bone	0.459	2178
Kidney	1.49	671
Intestinal fluid	100	10

This particular slice was chosen for display of the current density distribution because it is away from the tip of the dipole, and current flow from the dipole has enough space to spread out. However, any other slice would have been equally good as a representative slice for the display of the current density distribution. The plots are shown for the anisotropic and isotropic cases, and for the difference between the two. The upper row of the plots is for the whole slice and the bottom row of the plots is for a magnified view in the heart and surrounding areas. The maximum and minimum values of the contours and the separation, $\mathrm{d}j$, between the contour lines are given in the plots. The top plots have 80 contour lines in each plot between the maximum and minimum peak values, while the bottom plots have only 20 contours between the maximum and minimum peak values. For this reason the contour separation values, $\mathrm{d}j$, for the top and bottom row of plots are different.

The current density distribution for the anisotropic myocardium shown in the bottom left plot has more structural pattern than the isotropic case shown in the bottom middle plot. Both plots are remarkably different. The contour lines seem to be almost circular for the isotropic case with one noticeable peak in the centre. For the anisotropic case there seem to be many peaks and valleys. These are more recognizable in the difference plot at the bottom right. The difference between the anisotropic and isotropic case shown in the top right and bottom right plots seems to show a pattern of current distribution similar to the anisotropic case. This would suggest that in the vicinity of the heart the current flow pattern is significantly influenced by the myocardial anisotropy. In the difference plot, the positive contour lines are shown with solid lines and the negative ones with dashed lines. The current density distribution has distinct contour lines at some of the tissue boundaries. This is expected because at some of the tissue boundaries the resistivity values are significantly different from one another, which will change the current flow in a very noticeable fashion. Examples of these are the spinal column and the surrounding tissues, and at the boundaries of lungs, fat, bone and muscles. It is more noticeable in the difference plots. This implies that the difference plots are more dominated by the anisotropic current density distribution than the isotropic one. The maximum and minimum peak values for the difference plots are: 0.84 and -0.44 μA cm^{-2} respectively. The separation between the contours is $\mathrm{d}j = 0.0162$ μA cm^{-2}. The details of the difference of the current

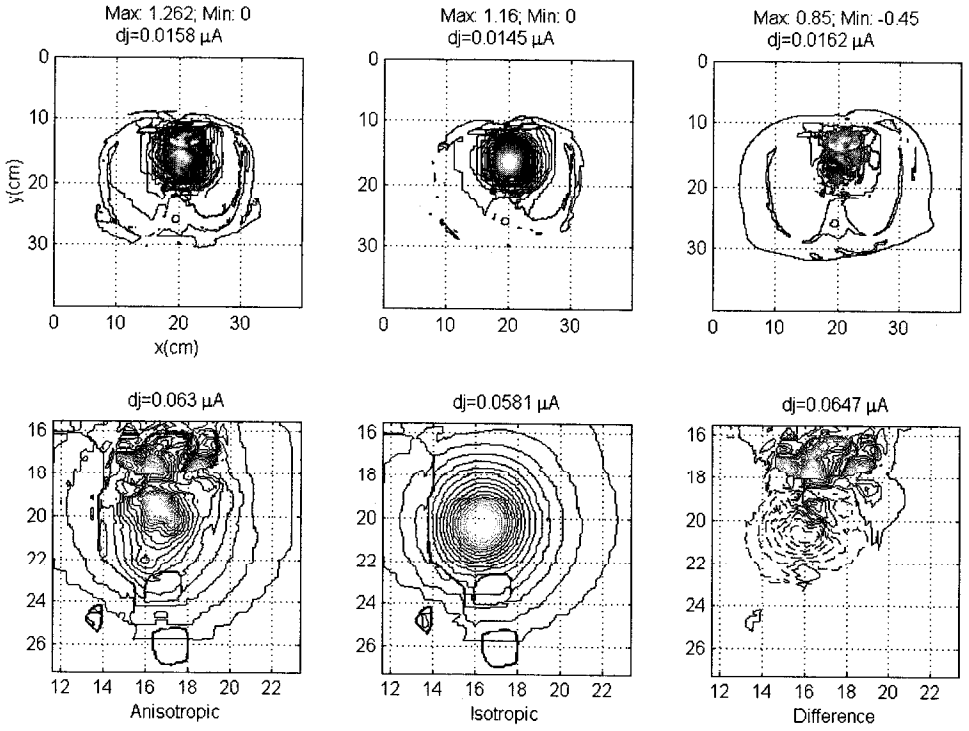

Figure 2. Contour plot of the current density distribution in one of the image slices. Top row: plots for the whole torso slice; bottom row: plots for the details in the heart area. Plots are for the anisotropic, isotropic and the difference between the two cases.

density distribution in the heart area are given in the magnified views in the bottom right plot. The contours are plotted with $\mathrm{d}j = 0.065\ \mu\mathrm{A\ cm}^{-2}$. Due to the myocardial anisotropy in the heart wall, the differences in the current distribution are more pronounced and complex than in the other areas of the torso.

To quantify the differences, the correlation coefficient between the anisotropic and isotropic current density distribution was computed. For the current density distribution shown in figure 2 it is 0.92. The correlation coefficient provides a degree of measure to compare the two quantities. A unity value of the correlation coefficient signifies that two quantities are the same, and a zero value would suggest that they are totally different. Thus, a correlation coefficient of 0.92 would suggest that the current density distribution shown in figure 2 is different with very noticeable contour patterns.

The correlation coefficients for other slices were also computed, and these are plotted in figure 3. Slices containing the heart are marked in the figure. The correlation coefficients for the slices in the heart area have values in the range of 0.66 to 0.97, suggesting that the myocardial anisotropy influences the current flow very strongly within the heart and in the vicinity of the heart. Now, going away from the heart, either towards the upper chest area or the lower lungs and abdomen area, the correlation coefficient is in the range of 0.97 to 0.99. This would suggest that the current density distribution is slightly affected by the myocardial anisotropy in the torso areas away from the heart. One reason could be that isotropic conductivities of the other tissues in the upper and lower torso smooth out the anisotropy dependent current flow patterns coming out of the heart wall.

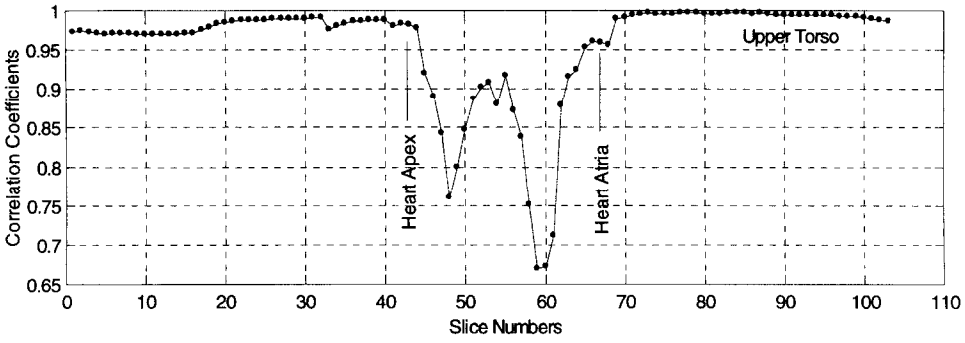

Figure 3. Correlation coefficients of the anisotropic and isotropic current density distribution for all the slices of the torso model. Slices going the through the heart are identified. The plot shows that the correlation coefficient for slices in the heart area is low, implying that the anisotropic and isotropic current distributions are very different from each other.

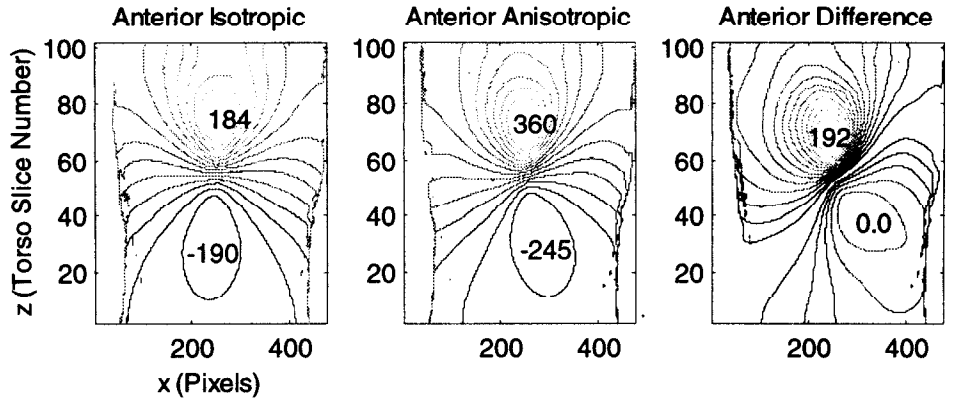

Figure 4. Contour plots of the anterior body surface potentials for the isotropic, anisotropic and the difference between the two. All values are in microvolts.

3.2. Body surface potentials

Contour plots of the body surface potentials are shown in figure 4. These are for the front (anterior) torso surface only. The left-hand contour plot is for the isotropic case, the middle contour plot is for the anisotropic case, and the right-hand contour plot is for the difference of the two. The horizontal axis is in image pixels and the vertical axis is in slice numbers. The slice thickness in our model is 0.3 mm which can be used to convert the slice numbers to the actual values in centimetres. The correlation coefficient of the anisotropic and isotropic contour plots is 0.96, signifying that the two plots are noticeably different from each other.

The maximum and minimum values are also given in the plots. The maximum and minimum values for the isotropic case are 184 μV and -190 μV; for the anisotropic case they are 360 μV and -245 μV. The location of the maximum and minimum contours is slightly different for the isotropic and anisotropic cases. This is more recognizable in the difference plot where maximum and minimum values are 192 μV an 0.0 μV respectively. From these figures one could infer that myocardial anisotropy does influence the body surface potentials.

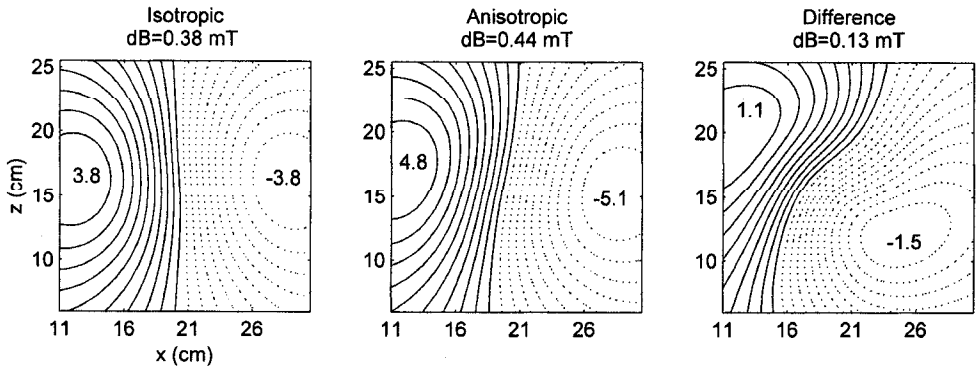

Figure 5. Contour plots of the normal component of the magnetic field for the isotropic, anisotropic and the difference between the two. There are only slight noticeable differences between the isotropic and the anisotropic contour plots.

3.3. Torso magnetic field profiles

Figure 5 shows the contour plot of the y component (~normal to the torso) of the magnetic field in a planar sampling surface. It shows the field plot for the isotropic, anisotropic and the difference of the two plots. The positive contours are shown with solid lines and the negative contours with dotted lines. The maximum and minimum peak values, and the separation between the contours, dB, for all three plots are given. The contour plots show a pattern similar to the magnetic field of a dipolar source which are characterized by the symmetrically placed positive and negative contour peaks with respect to the zero crossing line. This fits well because the source is a dipole oriented in the z direction, and thus the y component of the magnetic field will be similar to the contour plot of a dipolar source.

The correlation coefficient of the anisotropic and isotropic magnetic field profiles is 0.98. This would suggest that the anisotropic and isotropic magnetic fields are only slightly different from each other with some noticeable differences in the contour patterns. The zero-crossing contour lines are almost vertical for the isotropic case, while for the anisotropic case they are slightly tilted towards the right. These features are more pronounced in the difference contour plot. The maximum and minimum peak values are also different for the two cases. The maximum and minimum peak values for the isotropic case are 3.8 mT and -3.8 mT respectively. For the anisotropic case the maximum and minimum peak values are 4.8 mT and -5.1 mT respectively. The difference contours have maximum and minimum peak values of 1.1 mT and -1.5 mT. Note that the spatial locations of the peaks are at slightly different positions for isotropic, anisotropic and the difference magnetic field plots. In general, the differences between the isotropic and anisotropic cases are recognizable.

4. Discussion

These results show that myocardial anisotropy influences the current flow pattern very strongly in the heart and in the surrounding tissue areas. Away from the heart, for instance in the upper torso area and in the lower lungs and abdomen area, the current flow is not very strongly affected by the myocardial anisotropy. One reason could be that the volume conduction away from the heart smooths out the anisotropy-dependent current flow emanating from the heart area. The differences in the current density distributions are very noticeable in the heart area, which could

certainly be attributed to the myocardial tissue orientation. The differences are also noticeable at the tissue boundaries in the torso. Body surface potentials also show noticeable differences which arise due to the anisotropy-dependent changes in the torso current flow patterns. These results would suggest that myocardial anisotropy should be included in anatomically realistic models of the heart and torso for computer modelling of the electrical activity of the heart.

The torso magnetic fields show some noticeable but not very large differences. Even a slight difference in the magnetic field profile would influence the localization of the sources while solving the biomagnetic inverse problem. It has been observed before that a correlation coefficient of 0.98 will yield an average localization errors of 0.5 to 0.8 cm and a maximum localization error of up to 1.5 cm (Haueisen *et al* 1999, Jazbinsek and Hren 1999).

Here we have used a highly heterogeneous model of the heart and torso which provides a very good account of the current flow patterns in the torso. We have used similar models before to analyse the volume currents in the torso (Czapski *et al* 1996) and computer simulation of MCGs (Ramon *et al* 1998). The anisotropy in the myocardium was interpolated from the dog heart data which is the best can be done given the current state of knowledge. Thus our heart torso model is very accurate in analysing the effect of myocardial anisotropy on body surface potentials and magnetic fields. We have used a single dipole in the middle portion of the septum of the heart wall. This does not represent the myocardial activation sequences for modelling the QRS complex. This idealized representation of the dipole is just used as a source to analyse the effect of myocardial anisotropy. Our results should be considered as preliminary ones. These findings should be further extended by placing the dipoles in different parts of the myocardium as well as simulating the ECG and MCG waveforms. In summary, these results do show that the myocardial anisotropy changes the current distribution in the torso very significantly, and the resultant body surface potentials and torso magnetic fields also show related changes.

Acknowledgments

This research was partially supported by a National Science Foundation grant number INT-9726712 and an NIH grant number RR13301-01, and an equipment grant from the Seattle Foundation.

References

Czapski P, Ramon C, Huntsman L L, Bardy G and Kim Y 1996 On the contribution of volume currents to the total magnetic field resulting from the heart excitation process: a simulation study *IEEE Trans. Biomed. Eng.* **44** 95–104

Czapski P, Ramon C, Haueisen J, Huntsman L L, Nowak H, Bardy G H, Leder U and Kim Y 1998 MCG simulations of myocardial infarctions with a realistic heart–torso model *IEEE Trans. Biomed. Eng.* **45** 1313–21

Eason J, Schmidt J, Dabasinskas A, Siekas G, Aguel F and Trayanova N 199 Influence of anisotropy on local and global measures of potential gradient in computer models of defibrillation *Ann. Biomed Eng.* **26** 840–9

Foley T A 1995 Deformation of volumes using scattered landmark points *Intelligent Systems: Third Golden International Conference – Edited and Selected Papers* ed E A Yfantis (Norwell: Kluwer) pp 841–51

Foster K R and Schwan H P 1989 Dielectric properties of tissues and biological materials: a critical review *CRC Crit. Rev. Biomed. Eng.* **17** 25–104

Geddes L A and Baker L E 1967 The specific resistance of biological material *Med. Biol. Eng.* **5** 271–93

Haueisen J, Bottner A, Nowak H, Brauer H and Weiller C 1999 The influence of conductivity changes in boundary element compartments on the forward and inverse problem in electroencephalography and magnetoencephalography *Biomed. Eng.* **44** 150–7

Huiskamp G 1998 Simulation of depolarization in a membrane-equation based model of the anisotropic ventricle *IEEE Trans. Biomed. Eng.* **45** 847–55

Jazbinsek V and Hren R 1999 Influence of randomly displaced BSPM leads on the identification of ventricular preexcitation sites *Biomed. Eng.* **44** (suppl 2) 104–7

Lorange M and Gulajani R M 1993 A computer heart model incorporating anisotropic propagation. I. Model construction and simulation of normal activation *J. Electrocardiol.* **26** 245–61

Nielsen P M F, Le Grice I J, Smaill B H and Hunter P J 1991 Mathematical model of geometry and fibrous structure of the heart *Am. J. Physiol.* **260** H1365–78

Plonsey R 1974 An evaluation of several cardiac activation models *J. Electrocardiol.* **7** 237–44

Ramon C, Czapski P, Haueisen J, Huntsman L L, Nowak H, Bardy G H, Leder U, Kim Y and Nelson J A 1998 MCG simulations with a realistic heart–torso model *IEEE Trans. Biomed. Eng.* **45** 1322–41

Rush S, Abildskov J A and McFee R 1962 Resistivity of body tissues at low frequencies *Circ. Res.* **12** 40–50

Schimpf P H, Haynor D R and Kim Y 1996 Object-free adaptive meshing in highly heterogeneous 3-D domains *Int. J. Biomed. Comput.* **40** 209–25

Schimpf P, Haueisen J, Ramon C and Nowak H 1998 Realistic computer models of electric and magnetic fields of human head and torso *Parallel Comput.* **24** 1433–60

Schmidt J A and Pilkington T C 1991 The volume conductor effects of anisotropic muscle on body surface potentials using an eccentric spheres model *IEEE Trans. Biomed. Eng.* **38** 300–3

Siregar P, Sineteff J P, Julen N and Le Beux P 1998 An interactive D anisotropic cellular automata model of the heart *Comput. Biomed. Res.* **31** 323–47

Streeter D D Jr 1979 Gross morphology and fiber geometry of the heart *Handbook of Physiology: A Critical, Comprehensive Presentation of Physiological Knowledge and Concepts* vol 1, ed R M Berne (Bethesda, MD: American Physiological Society) pp 61–112

Taccardi B, Lux R L, Ershler P R, Macleod R, Dustman T J and Ingebrigtsen N 1997 Anatomical architecture and electrical activity of the heart *Acta Cardiol.* **52** 91–105

Thivierge M, Gulrajani R M and Savard P 1997 effects of rotational myocardial anisotropy in forward potential computations with equivalent heart dipole *Ann. Biomed. Eng.* **25** 477–98

Wang Y 1999 Analysis of defibrillation efficacy and investigation of impedance cardiography with finite element models incorporating anisotropic myocardium *PhD Dissertation* University of Washington, Seattle

Wei D, Okazaki O and Harumi K 1995a Comparison of body surface potential maps simulated with isotropic and anisotropic computer heart models *J. Electrocardiol.* **28** 346–7

Wei D, Okazaki O, Harumi K, Harasawa E and Hosaka H 1995b Comparative simulation of excitation and body surface electrocardiogram with isotropic and anisotropic computer heart models *IEEE Trans. Biomed. Eng.* **42** 343–57